Beam pattern (diffraction) aspects in design of the SPIRE instrument.

Martin E Caldwell[a*], Bruce M. Swinyard[a], Anthony G. Richards[a], Kjetil Dohlen[b].
[a] Rutherford Appleton Laboratory, Chilton, Didcot, OX11 OQX, UK.
[b] Laboratoire d'Astrophysique de Marseille, 2, Place Le Verrier, 13248 Marseille Cedex 4, FRANCE

Keywords: Diffraction, long wavelength, sub-millimetre, stray-light, quasi-optics.

1. ABSTRACT SPIRE-RAL-PUB-000372

In optical instruments incorporating longer IR wavelengths we begin to find (1) The wavelength is no longer a negligible fraction of the aperture (beam) width. (2) The detectors used have specific spatial coherence properties.

As a result the diffractive nature of beam propagation becomes important, and the main optical design tool of geometric ray-tracing has to be supplemented by quasi-optics (beam-mode) or finite element techniques.

These long wavelength aspects affect the instrument performance mainly in :-
1. Instrument field-of-view response or point spread function (PSF) pattern is no longer controlled by single pupil & field stops alone, but by several components.
2. The stray-light is increased.
Both of these arise because clipping of the beam by additional optical components is unavoidable, and the trade-offs in spatial resolution & stray light (edge-diffraction) must be managed, e.g. using non-standard Lyot stop arrangements.

In SPIRE these features arise because the amount of instrument functionality (& so complexity) which must be fitted within a finite available space drives down the aperture sizes relative to wavelength. However the wide spectral range means that these long wavelength performance features must be carefully balanced against the shorter wavelength requirements in the overall system design.

We report on these aspects of the SPIRE design, with beam simulation examples from trade-off studies on Lyot-stop design, and end-to-end computations of instrument field-of-view response.

2. INTRODUCTION.

The photometer and fourier transform spectrometer that comprise the SPIRE instrument both operate over a broad wavelength range (~ 0.2 to 0.7mm). They are both imaging systems (the FOV's are respectively 8x4 arcminutes and 2.6 arcminutes diameter), wherein the beams are relayed through several stages of imaging before reaching the detector. As well as the 'functional' components in the optical path, i.e. powered mirrors, windows, stops, filters & the interferometer delay path, there are also several flat mirrors, used to fold the beam into the available space.

Due to the constraints of the instrument size, this degree of complexity forces the instrument pupil size to be 'limited' in terms of its diameter in number of wavelengths. At the cold stop the pupil has diameter D≈20mm , i.e. at λ=0.7mm , D/λ ~ 30 wavelengths.

This, combined with the need to keep the relative aperture of the beams to F > 4 (for folding and component performance), means that the diffractive aspect of the beam propagation becomes significant. For example, the co-focal beam parameter $z_0 = 4.\lambda.F^2/\pi$ is >16mm for the above values, and is therefore not negligible compared to the separations of the powered mirrors (typically ~ 150 mm). As a result, the principles of *Geometric Optics* (GO, i.e. the imaging equations on which ray-trace programs are based), which apply as D/$\lambda \rightarrow \infty$, are no longer sufficient to describe all aspects of optical performance.

In this regard, the analysis methods of long-wave optics may be used, and these are well developed for the mm-wave field[1]. Indeed the SPIRE instrument operates in a range of D/λ where the two 'traditions' of optical & mm-wave design are

* Correspondence: E-mail m.caldwell@rl.ac.uk Tel.(44) 1235 446586.

merging. However, because in SPIRE these effects are only large at the long-wavelength extreme of a broad wavelength range, and because it is an imaging instrument made up of many components, the optical analysis methods are still the more appropriate[2]. Therefore the optical design of SPIRE is essentially based on GO methods (the design is presented elsewhere in this volume[3]). Supplementary long-wavelength analyses are needed to cover the following aspects, which are the subject of this paper :-

1. Interferometer performance: diffractive beam divergence and shape.
2. λ- dependent imaging aberrations: a reflective system designed for shorter wavelengths degrades as it is used at longer wavelength.
3. Beam shape effects. In GO the beam would have uniform intensity in all non-focal plane locations, and the detector would be incoherent. In SPIRE the detectors (feed-horns) have their own spatial coherence properties, i.e. beam-shape, and this must be propagated through the system to investigate beam clipping (stray-light), instrument FOV& imaging properties.

3. THE LONG-WAVELENGTH EFFECTS IN SPIRE.

1. Beam shape (non-imaging aspects).

In this paper we use the term 'beam' to refer to a coherent wavefront . This may be an incoming 'signal beam' from a single point source on the sky, or an outgoing 'detector beam', from a single spatial mode of the detector feed-horn, & propagated in a 'time-reversed' sense[1]. Many long-wave optics systems are of the non-imaging type, i.e. they use a single detector (beam) rather than an array of detectors, so we will consider the non-imaging aspects first.

The detector beam is often a lowest-order mode which approximates to a gaussian beam, a form simple to analyse & so used in first-order design, where in addition the powered mirrors are approximated to thin lenses. The coupling of the detector beam field ψ_d to the signal beam ψ_s , i.e. that from the distant point source, is described by the *aperture efficiency* , which is a spatial overlap integral (inner product) over a section perpendicular to the optical path. In terms of intensity detection this efficiency is [4]

$$h = \left|\left\langle y_s \middle| y_d \right\rangle\right|^2 \qquad (1)$$

where the inner product is $\left\langle y_s \middle| y_d \right\rangle = \iint y_s^*(x,y,z).y_d(x,y,z).dx.dy$

and each field is normalised so that its self inner product is equal to 1. It is usually calculated at the plane of the detector horn aperture as shown in fig.1.

Although the detector beam usually has certain polarisation properties, the source is assumed unpolarised & so the scalar (rather than vector) fields are relevant here. In choosing the detector/ system aperture sizes there is a trade-off between the need for the detector beam to adequately fill the telescope aperture, but for not too much of it to spill over the edges. In SPIRE both bare and feed-horn detectors have been considered & the latter chosen for sensitivity reasons. For a corresponding gaussian detector beam, and Airy-pattern signal beam, the maximum efficiency is $\eta \approx 80\ \%$ [5], occurring near a detector waist size of $w_d = 2F\lambda/\pi$ (approx. 1/e amplitude edge taper at a system exit pupil of relative aperture F). The detector size (horn aperture diameter) is chosen to be $2F\lambda$, i.e. close to the Airy disc size, and the pixels are close-packed such that their spacing is $s \approx \pi w_d$. This would give under-sampling of images with respect to the optimum resolution ($s \approx w_d$), but SPIRE uses scanning of its FOV to improve the sampling.

For a more detailed analysis the detector beam is described using higher order gauss-hermite beam-modes, to include effects such as real detector beam-shape, aberrations & clipping. Beam-modes are used because their propagation & imaging can be described using Fourier Optics. For broad-band systems this approach suggests a configuration in which wavelength-independent coherent imaging (of the beam waist) is obtained, by using powered components separated by distances equal to the sum of the focal lengths, as in the gaussian-beam telescope[6]. This also gives a beam pattern on the sky which is λ-independent, as is often desirable for remote-sensing applications. In the broad-band astronomy application however it is unsuitable because it leads to a fill-factor of the aperture which varies with wavelength, whereas the priority is for optimum fill factor (collection efficiency) across all wavelengths. Consequently in SPIRE we have image (waist) locations which

vary with wavelength, with the short-wavelength limit approaching the GO focus. This waist deviation from GO focus is not cumulative, i.e. it does not increase with number of imaging stages. The long-wavelength effects which result include:

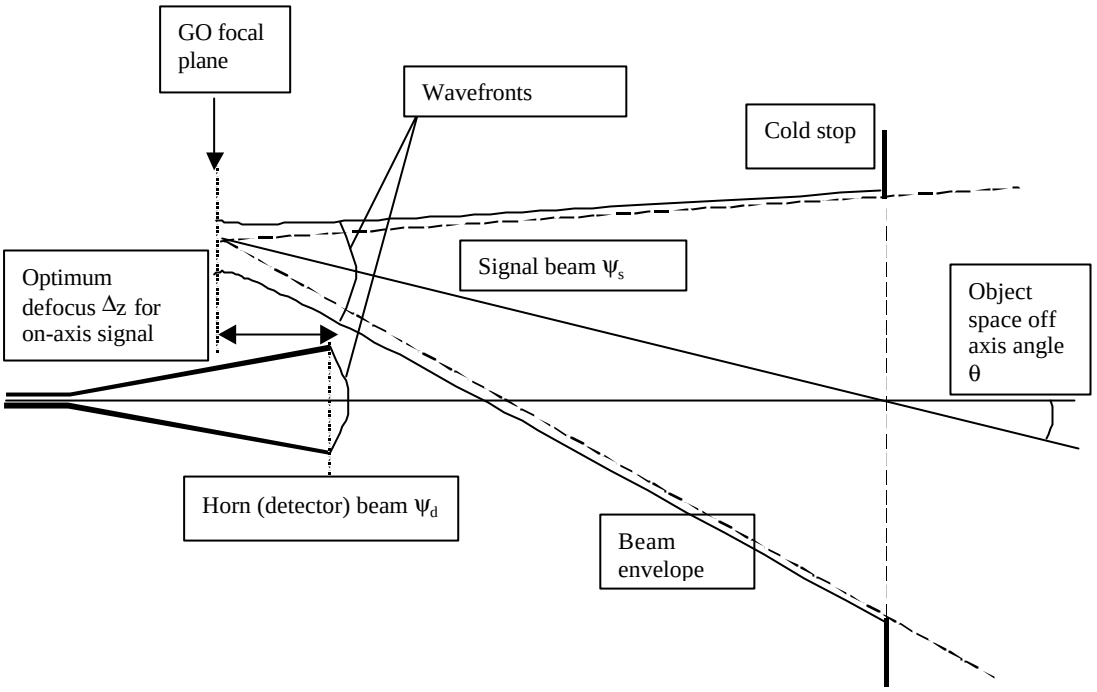

Figure.1. Beam geometry for calculation of efficiency.

1. Long-wavelength 'defocus'. The signal beam final focus varies with λ. In the photometer this can be compensated channel-by-channel since a different detector arrays is used in each. In the spectrometer however, it means that some drop in efficiency must arise at the band edges. Fig.2. illustrates this effect. Here for analysis the optical path is 'unfolded' and only the powered mirrors represented, as thin lenses. The long wavelength defocus is calculated through the system[7], and is found to be ΔZ=3.7mm at the detector for λ=0.5mm.
2. Long-wavelength coma aberration. The powered mirrors are conic surfaces, which at short wavelength relay the image (& beam waist) between the mirror's geometric foci with low aberration. At long wavelengths the defocus effect upsets this scheme, leading to coma aberration[8]. In our example in fig.2 this amounts to < λ/400 wavefront error at the beam edge, per component, so the effect is small in SPIRE, but if the system were used at e.g. λ=5mm it would rise to < λ/15 per component.
3. The interferometer collimated beam, being actually a diffraction-limited divergent beam, could show long wavelength defocus effects due to powered optics being placed between the splitter & recombiner. In fact providing these optics are symmetrical in each arm, as they are in SPIRE (fig.2a), the defocus occurs equally in each arm & there is no first-order effect.

The beam shape is also an important feature of the FTS interferometric efficiency (fringe visibility). At low optical path difference (OPD) the visibility is high regardless of beam shape, and its decrease at larger OPD, due to the well-known diffractive apodisation effect, depends on the beam shape & sets a minimum aperture required to achieve a given resolving power[9]. For a gaussian beam model SPIRE has w=15mm, and at λ=0.5mm and maximum OPD=125mm the wavefront mismatch (due to curvature difference) is <λ/100, which is acceptable in the performance budget.

When we consider off-axis detectors (non-zero FOV), we have the additional effect of pupil lateral shift with mirror travel, equivalent to angular misalignment of the beams interfering at the detector. For beam shape, wavelength & OPD as above this gives a reduction in contrast by 15 % when the FOV radial position is increased from 0 to 1 arcminute.

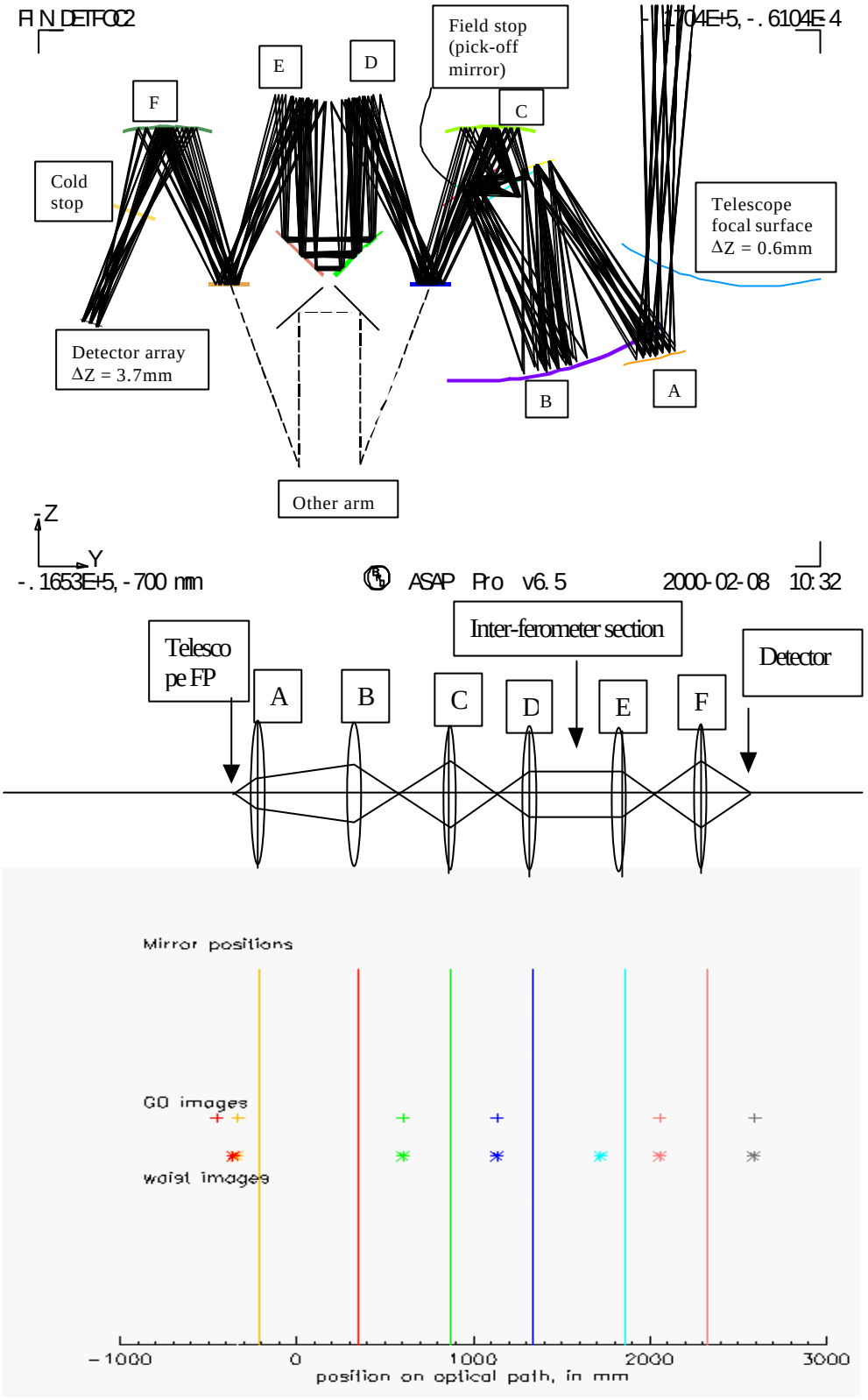

Figure 2. FTS optics ray-trace, equivalent unfolded imaging system, and plot of image positions, for case λ=0.5mm. The input beam waist is positioned co-incident with the GO focus of the telescope primary mirror, and its offset from GO focus at subsequent focal planes is labeled Δz in the ray-trace.

2. Imaging aspects.

When imaging is required, i.e. handling of an array of beams defining a FOV, each individual conic section mirror cannot be aberration free over the FOV even at short wavelength, and its aberrations increase with FOV size. Good beam quality , as expressed for example by the Strehl ratio, can be provided over an extended FOV by using combinations of conics that can cancel each other's aberrations, and indeed in the optics tradition this is the subject of GO-based design of reflective systems to produce wide-angle imaging using 3 or 4 mirrors. This GO design task would become still more complicated if the long-wavelength aspect were to be included, but in SPIRE the effects are sufficiently small (as above), the wavelength range broad & the FOV narrow, that the GO design method is adequate[3].

However there is an additional imaging design constraint, arising from stray-light considerations at longer wavelengths, and this concerns aberration in the imaging between pupil planes. In SPIRE stray-light sources are present particularly in thermal emission from the warmer enclosures surrounding pupils nearer the front of the instrument, and this can reach the detector via beam clipping (edge-diffraction). In order that the detector beam as clipped by the cold stop doesn't see a significant part of these warmer forward pupil edges, the cold stop must be undersized with respect to them, by an amount which depends on the build tolerances and the quality of imaging between these pupils. In order to maintain reasonable throughput it is therefore required that the pupil aberration be kept small, e.g. to < 5 % of radius.

3. Beam clipping.

Where the beam edges are truncated or 'clipped' by the finite apertures of components, the main effects on performance are: 1. Increased susceptibility to stray-light , both from on-board emissions and from 2. Increased side-lobe levels on the instrument's FOV response function[2]. In this regard long-wavelength systems often strive to have all component apertures oversized several times with respect to the detector beam, to keep this unclipped throughout the system and so preserve its gaussian (zero side-lobe) shape.

In SPIRE however, the need to fill the telescope aperture means that some overspill i.e. clipping of the detector beam is required, and for low stray-light this is best implemented at a cold stop, i.e. close to the cooled detector . For flat-fielding of the array response this should also be a pupil plane in the GO sense, i.e. the same clipping for all detectors making up the image. Ideally all of the other components (including the telescope pupil at M2) should then be *oversized* with respect to the resulting beam, to avoid any additional diffracted stray-light. For a telescope of fixed pupil size, this actually means an *undersize* of the instrument beam, and this approach is that of the classical Lyot stop[10]. In instruments for the thermal IR region the undersize required for efficient stray-light blocking is in the region of 1 % [11], but at the SPIRE longer wavelengths the required undersize is approx. 15 %, an amount which is prohibitive because it would reduce the throughput, (by approx. 30%) at all wavelengths (section 5).

Likewise the oversize of other components relative to the instrument beam cannot always be made large, but calculations of beam patterns at the various components show that at most far-field (i.e. non image plane) components in SPIRE, an oversize of 20 % with respect to the geometric shadow (as defined e.g. by the rays of fig.2), is sufficient to give low stray-light, at least for the on-axis (zero FOV) beam. A notable exception in figure 2 is the interferometer collimating mirror 'D', which cannot be oversized in the region where it is adjacent to mirror 'E'. In this case the spillover of the long wavelength beam from D onto E is reflected at sufficient angle to the wanted beam that it can be trapped, on a baffle surface inserted between mirrors E & F.

So it is that in SPIRE the clipping of the beam at multiple components, and the associated increased stray-light at long wavelength, has been an accepted part of the broad-band design[2]. Indeed the bottom line for the above long-wavelength effects is that the GO design gives adequate performance in the short-wavelength, centre-of-FOV case, and the degradations which become significant at the long-wavelength end of the range, and outer detectors of the FOV, have to be accepted as unavoidable if the design is to be broad-band with throughput as a performance priority.

4. BEAM SHAPE CHARACTERISTICS.

The detector for SPIRE is to be a bolometric sensor within a feed horn which has a circular cross-section and aperture diameter d sized to match the signal beam Airy disc diameter at the design wavelength λ_{des}, i.e. $d = 2.F.\lambda_{des}$. Our work to date has been for smooth-walled conical horns which propagate modes (as per a circular waveguide[12]) having distinct patterns & mixed polarisation, where the fundamental mode (TE_{11}) approximates in scalar terms to a truncated gaussian with astigmatism. However SPIRE may use corrugated feed-horns, and in that case the fundamental mode has a more symmetric gaussian-like shape and is plane-polarised[13].

(a)

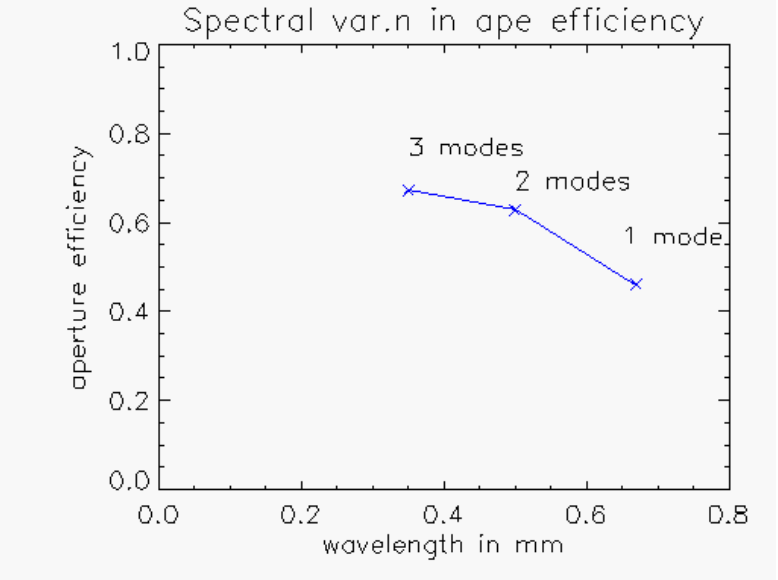

(b)

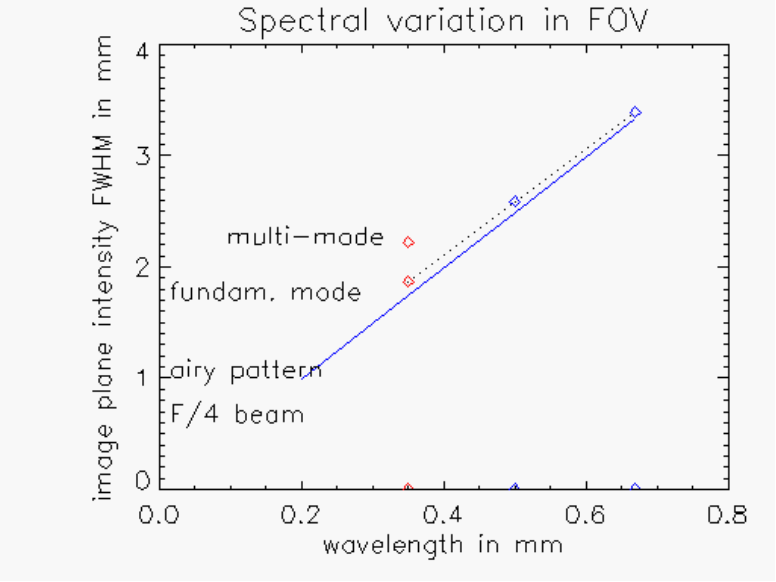

Figure 3. Spectral variations for broad-band horn design. (a) Aperture efficiency. (b) FOV width in FWHM averaged over 2 profiles , as per fig.4. NB Plot is at 3 wavelengths only, & does not show the mode cut-off wavelengths.

In this section we use the smooth-wall conical horn design for an example calculation of : 1. The beam pattern on some components in the system. 2. The instrument FOV response function (intensity beam pattern on the sky). The propagation method used is described elsewhere[2,14]

1. Patterns of a broad-band detector for spectrometer.

We consider the characteristics of a detector designed to cover the longer-wavelength part of the spectrometer band, i.e. 0.3 to 0.67mm. This has its entrance aperture sized at $2F\lambda$ for a design wavelength of λ_{des}=0.35mm, and in order to pass a mode up to the longest wavelength its exit (& connecting waveguide) aperture is made larger than would be the case for a narrowband design. As a result the horn is multi-moded, passing 1 & 3 modes at wavelengths of >0.5 and 0.35mm respectively. (In contrast the photometer has separate detectors for each of the 3 wavelength channels, and each of these is separately optimised for single-moded operation over a narrower band).

Figure 1 shows schematically how the finite length of the horn leads to some wavefront curvature at its aperture, and as a result some defocus Δz is necessary to optimise the efficiency, since this is a trade-off between the wavefront & amplitude overlaps in the integral equation (1). The optimum Δz, and efficiency loss relative to the perfect ($L=\infty$) case, both increase with wavelength, and in the SPIRE case of λ_{des}=0.35mm, L=30mm, their values are 2.5mm & 3 %.

For the beam-pattern the multi-mode aspect raises the question of how the individual modes sum to give the net beam pattern. The multi-mode detector beam has intensity given by the sum of the individual mode intensities with equal weights, under the assumptions that the detector is an ideal bolometer (energy sensor), & that its sensitivity, and the losses in the waveguide, are independent of wavelength and mode number. Calculation of the aperture efficiency as per equation (1) then gives a result which is equal to the average of the individual mode efficiencies. As a result the efficiency doesn't change greatly with the number of modes propagating, as figure 3a shows. The reducing efficiency at longer wavelengths is due to the signal beam Airy disc at the horn mouth becoming oversized with respect to the detector beam, whose amplitude pattern at the horn is independent of wavelength.

The complexity of the mode patterns (asymmetry & non-plane-polarised properties) cannot be fully shown here, and we just plot profiles of the patterns in directions within & normal to the symmetry plane of the system (i.e. the plane of fig.2). These profiles are shown in figure 4 for the cold stop & field stop (pick-off mirror image plane) of figure 2, while the width of the latter (in terms of FWHM) is also shown plotted versus wavelength in fig.3b. This beam width parameter is important as it is indicative of the FOV response on the sky, since each image plane is conjugate with the object (sky) plane (see next section).

We see in fig.4 that at λ_{des}=0.35mm the fundamental mode is clipped by the cold stop at approx. 0.1 to 0.2 in intensity, i.e. close to the $1/e^2$ 'edge taper' level of the gaussian beam sized for optimum efficiency in the first-order design. At the field stop this clipped beam has become somewhat wider than the Airy pattern for this stop size (fig.3b), due to the pupil edge taper, and the overall (3-mode) pattern at this wavelength is wider still.

At the long wavelength (0.5mm) in figure 4 the fundamental mode beam pattern fills the cold stop rather more (edge taper ~ 0.3 to 0.5, due to horn aperture now being $< 2F\lambda$), and so after clipping it has a more top-hat like shape and therefore at the field-stop a shape & width which are closer to that of the Airy pattern.

In summary we note from figure 3 that this broad-band configuration gives maximum multi-mode efficiency at the design wavelength & a spatial resolution which is reasonably close to the ideal (airy pattern) case.

2. Instrument FOV response.

The above field-stop beam intensity pattern is closely related to the instrument FOV response function. An appropriate definition of this function is that of the point-source transmittance[15] (PST) which for coherent detection is equivalent to the variation of detected intensity, as given by η , with angle of incidence θ as in figure 1.

In long-wavelength antenna systems the FOV response is often taken as given directly by the detector beam pattern on the sky[6], and this is consistent with equation 1 as follows. The clipping of the detector beam at the cold stop is equivalent to its being multiplied by the signal beam at this pupil plane, since the latter has a top-hat shape at this location. Using Fourier Optics the resulting *amplitude* beam pattern in the far-field (on the sky) is then equivalent to the convolution of two far-field patterns, those of the signal (Airy pattern) and detector (gaussian-like) beams.

If we now consider the PST as evaluation of equation (1) over all off-axis angles, we find that in the approximation that the wavefronts are matched (minimal aberration) and that the signal beam form doesn't vary with source off-axis angle, the *amplitude* detection efficiency ($\sqrt{\eta}$ versus θ) also reduces to the convolution of signal & detector beams[2]. Therefore the far-field beam pattern in intensity, is approximately equal to the PST function.

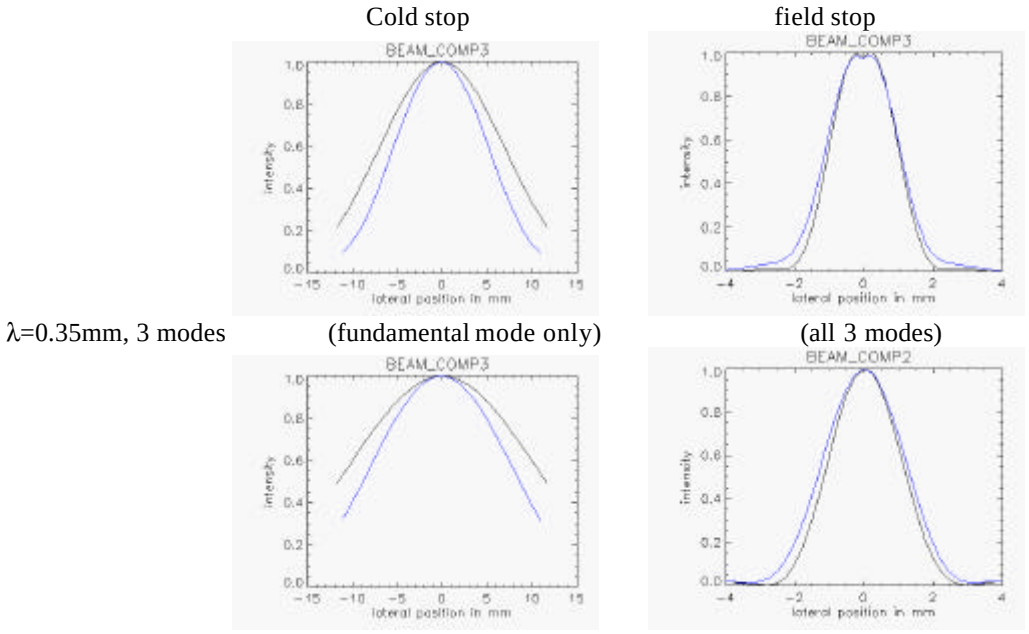

Figure 4. Beam modulus profiles at cold stop (left) and field stop (right), plotted versus position in mm, in 2 sections, parallel & perpendicular to plane of fig.2.

The full calculation of $\eta(\theta)$ is not included here, but the field stop beam patterns of figure 4 provide an approximate FOV response. The plotted horizontal scale, of position across the field stop, can be converted into equivalent far-field angle on the sky by multiplying by a factor $F_{tel}/(F_{fs}.f)$. Here F_{tel} and f are the f-number and focal length of the telescope and F_{fs} is the f-number of the beam at the field stop (pick-off mirror). In FIRST-SPIRE F_{tel} = 8.7, f=30.5metres & F_{fs}=4 . Such a conversion neglects any clipping or aberration of the beam which occurs between the field stop & object space. Clipping in the telescope is considered in the next section.

5. DIFFRACTED STRAY-LIGHT.

To investigate the Lyot stop issue, the long wavelength (0.5mm) beam is propagated outwards through the instrument to the telescope. Figures 5 & 6 show the instrument beam patterns for the case of a bare detector (i.e. without a feed-horn), of assumed size << $F\lambda$, such that the detector beam approximates to a uniform spherical-wave. When clipped by the cold stop this has a top-hat profile, i.e. edge taper ≈ 1, which is the worst-case for edge–diffraction. The detector beam pattern at the telescope focal plane is then close to an Airy pattern, and this is shown in figure 6a on a log scale, to emphasize how it is clipped by the rectangular field-stop aperture which defines the SPIRE field of view[3] at that plane.

The corresponding beam pattern at the telescope pupil M2, shown in profile in figure 6b, is a coherent image of that at the cold stop (instrument pupil), and so it should resemble a top-hat shape. However it can be seen that it actually has a rippled profile & a significant slope on its sides, and both of these features are diffraction effects associated with the clipping (& spatial filtering) of the beam pattern by the field stop. The edge slope is attributable to diffraction-limited resolution in the filtered image of the cold-stop edge, with a blur diameter for this imagery of

$$b \approx 2.F_{fs}.\lambda$$

where F_{fs} is the f-number for the angle which the field stop subtends at M2. In the example F≈50 giving b≈ 50mm, i.e. the edge-blurring is approx. 1/3 of the M2 aperture radius.

Figure 6b also shows how this beam pattern will be clipped by the edge of M2. In this example there is no undersizing of the cold stop relative to M2, & so the clipping is significant. (If a feed-horn detector beam were modeled , the clipping level would be reduced according to the pupil edge taper of that beam). The consequences of this significant clipping of the beam

by M2 are (1) The detector beam 'sees' the surround of M2. (2) Out-of-field radiance incident on the M2 edge can, by being diffracted there, enter the detector beam. An example of this is radiance emitted by the sun-shield.

In order to avoid the associated stray-light, the undersizing of the instrument cold stop should therefore include an edge-diffraction allowance, to make it an effective Lyot stop at long wavelength (i.e. the detector beam is made smaller to reduce its clipping by M2). However at this wavelength the diffractive undersize required is approx. half the blur diameter, i.e. 15 %, which would be unacceptable to the throughput requirement (affecting it across all wavelengths). An alternative might be to open up the field stop to reduce the blur diameter, but this is not possible due to the constraints from the other instruments & other stray-light requirements. It is therefore necessary to consider in greater detail whether the stray-light effects for a Lyot stop without diffractive undersizing could be acceptable.

For the view of the M2 surround, there is no problem because the spillover part of the beam simply views cold space at this wavelength (in an annulus or cone centred on the FOV, & of half-angle 3.2 degrees). Part of the surround is occupied by the spider legs, but these are reflective & have bevelled edges to also view to space.

For the edge-diffraction at the edge of M2, the main sources are thermal emission from the primary mirror M1 surface (ε=0.01, T=74K) and the inner surface of the telescope sun-shield (ε=0.04, T=170K), which lies on one side of the FIRST telescope as shown in figure 5. Edge-diffraction of the primary mirror emission is actually indistinguishable from the background signal due to this source already lying within the field-of-view, and it may be regarded as the contribution from the diffractive wings of the detector beam pattern (as clipped by M2) as it fills M1.

If the sun-shield had a similar emission to M1, its contribution would be equivalent to that from an extension of M1 on that side of the telescope. However, it has emissivity and black-body spectral radiance (at λ=0.5mm) which are higher than those of M1 by factors of 4 & 2.5 respectively, although it fills only approx. 1/3 of the telescope perimeter. The other parameter which is important to this edge-diffraction term is the off-axis distance across the used beam at which the transition from M1-to-sun-shield occurs. This is determined by (1) the M1 size relative to the pupil (M2) size, derivable from the telescope specifications of entrance pupil size (D=3.5m), entrance pupil distance from M1 (L=17m), unvignetted FOV radius (a=15 arcmin) and M1 radius oversize (o=17mm). (2) The instrument beam position, i.e. detector radial location r within the FIRST field of view.

In terms of distance x from the geometric shadow boundary, the edge occurs at x = o+(a-r).L, and for the worst-case outer corner of the SPIRE FOV (r=13.5 arcmins) , this gives x= 24mm. At this distance , emissivity & temperature the contribution from the sun-shield is found to be 0.2 % of the direct emission background from M1, and so for this design it is not a critical stray-light term.

In conclusion, it is found that for the FIRST-SPIRE system an instrument cold-stop with a diffraction undersize of zero, gives no serious long-wavelength stray-light threat. Undersize allowances for pupil aberration & mechanical tolerances are nevertheless still needed[3].

6. CONCLUSIONS.

We have found that the design of SPIRE as an optical imaging instrument, based on GO and with efficiency optimised across the wavelength range, leads to the following deviations in first-order (gaussian beam) performances at a longest design wavelength of 0.5mm:

- Gaussian waist position defocus at detector: < 4mm
- Long-wavelength coma: < λ/400
- Interferometer long-wavelength apodisation at max. OPD of 125mm : < λ/100.
- Contrast reduction at edge of FOV (1arcmin) & max. OPD : 15 %

As an example of more detailed analysis of beam shape effects, the case of a broad-band smooth-walled conical feed-horn was given and found to show reasonable (multi-mode) efficiency and FOV width close to diffraction limit over the band. These characteristics are inputs to the instrument performance studies to finalise the choice of detector design.

In most components an oversize of 20% relative to the GO beam is found to be sufficient with regard to maintaining the beam shape (1/e edge taper at cold stop), and keeping edge-diffracted stray-light minimal, at the centre of FOV. However the effects of the associated beam-clipping on instrument far-field beam pattern on the sky (e.g. added side-lobes), and degradation at the edge of FOV, have not been detailed.

Regarding the beam-shape relations between SPIRE & the FIRST telescope , it is found that edge-diffraction undersizing of the SPIRE pupil to avoid long-wavelength clipping at the FIRST pupil (i.e. Lyot stopping) is unattractive because it limits throughput at all wavelengths. The alternative of a SPIRE pupil with no undersize allowance for diffraction is acceptable from the stray-light viewpoint; its main consequence is long-wavelength spillover from the edge of telescope M2 onto the sky at 3.2 degrees from the line of sight.

7. ACKNOWLEDGEMENTS

The authors acknowledge the help of D Coburn of Maynouth University for supplying the mode data, and the UK Particle Physics & Astronomy Research Council for financial support.

8. REFERENCES.

1. Martin, D.H and Bowen, J.W., "Long Wave Optics", IEEE MTT **41**, pp.1676-1690, 1993.
2. M Caldwell, P F Gray & B Swinyard. "Multiple beam clipping in far infra-red & sub-millimetre space instruments: ISO-LWS and FIRST-SPIRE." Proc. SPIE **Vol. 3426**. 1998.
3. K. Dohlen et al. "Optical design of the SPIRE instrument for FIRST" SPIE **Vol.4013** (this volume).
4. J.W.Lamb "Quasi-optical coupling of gaussian beam systems to large Cassegrain Antennas" Int. J. of IR & mm-waves**. 7**,pp.1511-1535, 1986.
5. J.A. Murphy. "Aperture efficiencies of large axi-symmetric reflector antennas fed by conical horns" IEEE Trans. AP-Vol.36, No.4 (1988)
6. Martin, R.J and Martin, D.H., "Quasi-optic antennas for radiometric remote-sensing", Electronics & Communications Engineering Journal (IEE), **8** (1), February 1996.
7. S.A.Self "Focussing of spherical gaussian beams" Appl. Opt. p.658, **Vol.22**,No.5 ,1983.
8. J.A.Murphy. "Distortion of a simple gaussian beam on reflection from off-axis ellipsoidal mirrors" International journal of infrared & MM-waves, **Vol.8**, No.9, pp. 1165-1187 , 1987.
9. D.H.Martin et al "Dispersive fourier transform spectroscopy for the range 1-30cm-1" SPIE **Vol.1575**, pp.21-29, 1991.
10. B. Lyot. Mon. Not. R. Astron. Soc. **Vol.99** p.580 (1939).
11. M Caldwell & P F Gray. "Application of a generalised diffraction analysis to the design of a non-standard Lyot-stop system for the 'High resolution Dynamics Limb Sounder' (HIRDLS) instrument". Opt. Eng. **Vol.36**, No.10, pp.2793-2808, 1997.
12. Markuvitz. *Waveguide Handbook*. section 2.3.p.66.
13. R.J.Wylde "Millimetre wave gaussian beam-mode optics and corrugated feed horns" IEE Proc., **Vol.131**, Part H, No.4, pp.258-262, 1984.
14. M Caldwell & P F Gray. "Test of a ray-trace method for field calculations in antenna systems design" . Int. J. of IR & mm-waves. **Vol.20**, No.2, pp.279-304. 1999.
15. E. R. Freniere R.D.Stern and J.W.Howard, "SOAR: a program for the rapid calculation of stray light on the IBM PC", SPIE **Vol.1331** pp.107-117 , 1990.

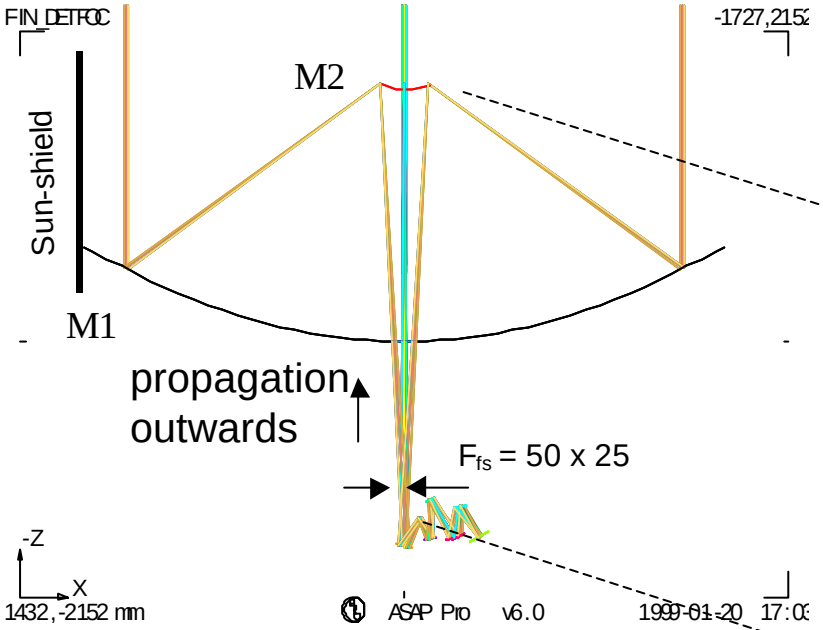

Figure 5. Telescope+PHOT layout. Y-direction points outwards from page.

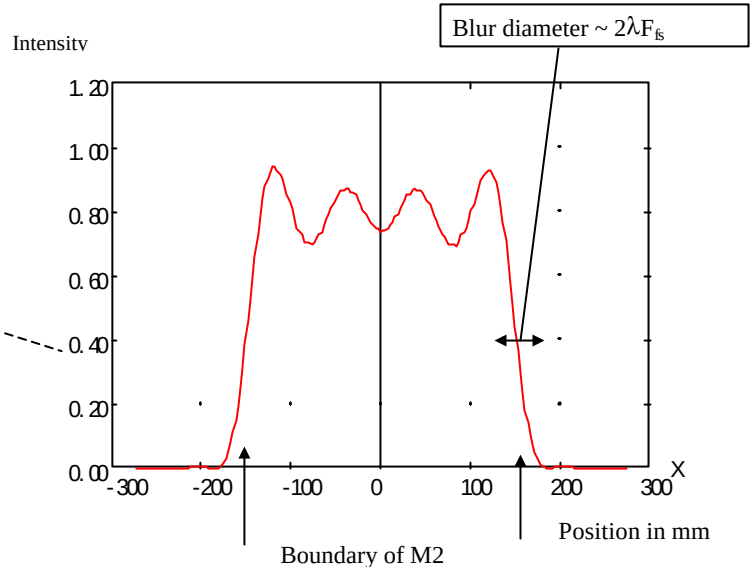

(b)

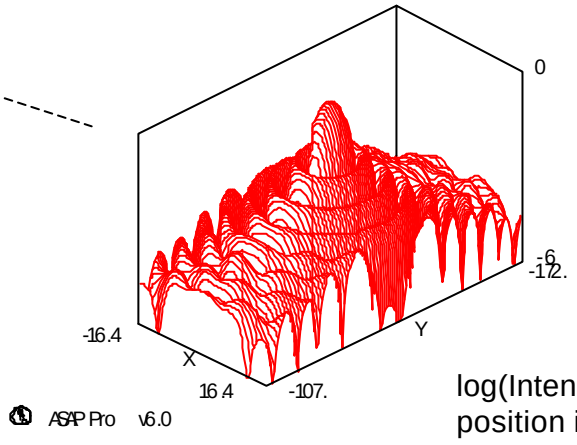

log(Intensity) vs position in mm

(a)

Figure 6. Detector beam patterns versus X – Y.